Does supramolecular ordering influence exciton transport in conjugated systems? Insight from atomistic simulations

T. A. Papadopoulos,[*,†] L. Muccioli,[*,‡] S. Athanasopoulos,[*,¶] A. B. Walker,[†] C. Zannoni,[‡] and D. Beljonne[¶]

Department of Physics, University of Bath, BA2 7AY Bath, U.K., Dipartimento di Chimica Fisica e Inorganica, Università di Bologna, IT-40136 Bologna, Italy, and Laboratory for Chemistry of Novel Materials, University of Mons, B-7000 Mons, Belgium

E-mail: tp239@bath.ac.uk; luca@fci.unibo.it; stavrosa@averell.umh.ac.be

Abstract

We present a theoretical platform for modelling temperature–dependent exciton transport in conjugated oligomers and we apply it to indenofluorene trimers. Atomistic MD simulations of these molecules confirm the experimentally observed occurrence of a liquid crystalline smectic phase at room temperature and predict a phase transition to the isotropic phase between 375 and 400 K. Strikingly, the increased orientational disorder at elevated temperatures does hardly affect the ability of excitons to move over large distances, though it affects the directionality of the energy diffusion process. Detailed quantum-chemical calculations show that this arises from a trade-off between reduced electronic couplings and increased spectral overlap at high temperatures.

[*]To whom correspondence should be addressed
[†]Department of Physics, University of Bath, BA2 7AY Bath, U.K.
[‡]Dipartimento di Chimica Fisica e Inorganica, Università di Bologna, IT-40136 Bologna, Italy
[¶]Laboratory for Chemistry of Novel Materials, University of Mons, B-7000 Mons, Belgium

Introduction

Tuning the electronic and excitonic transport properties in organic materials is a critical issue for the use of these materials in efficient optoelectronic devices, such as light emitting diodes,[1] field effect transistors,[2] chemical sensors[3] and solar cells.[4,5] Especially in the search for renewable energy resources, organic solar cells could be complementary to their inorganic counterparts, which until now have demonstrated significantly higher performances. Although there has been a considerable improvement on the efficiencies of organic devices in the last years, most advances are due to a rather unsystematic development of novel materials implemented in new architectures.[6] However, such efforts could be fragmented or even ill–directed in the absence of effective routes for predicting, rather than discovering, the optoelectronic properties of the materials. New materials result in new morphologies and physical properties,[7] and since progress and understanding run in tandem, tailoring the transport properties and improving the efficiency requires the description of both the morphological and electronic properties using physical models that retain the key atomistic details. So far, improvements on the efficiency of organic devices have been hindered due to a lack of detailed theoretical understanding of the combined effects of these two factors. This is partly due to the complexity of the materials involved and the large number of parameters in play. One way to overcome some of these difficulties by reducing the number of uncontrolled parameters is the oligomer approach.[8] Systems that are built up of single spectroscopic units and have well defined conjugation lengths, are in fact relatively free from chemical and structural defects and are amenable to higher orientational and/or positional order. It follows that the energy transfer in such controlled morphologies will benefit from small energetic disorder that is one of the main limitations of exciton diffusion.[9] Henceforth conjugated oligomers, due to their reduced complexity, could work as prototypes for validating theory through comparison with experiment.

The purpose of this paper is to provide a protocol for calculating exciton transport properties in

bulk conjugated materials and to test how sensitive the transport properties of oligomeric materials are to changes in the morphology and temperature. We employ methods from statistical physics and quantum chemistry that allow us to link the molecular parameters to the (opto)electronic properties. The morphological properties are evaluated with atomistic Molecular Dynamics (MD) simulations, while exciton transfer rates are directly evaluated from the chemical structure via correlated quantum-chemical calculations and transport properties are sampled with a kinetic Monte Carlo (MC) model. We can therefore directly calculate the exciton transport properties from the molecular structure avoiding any a priori assumptions on molecular conformations and packing.

The system chosen to validate the theoretical approach is an indenofluorene trimer (IF3) that has recently been studied experimentally and was shown to form smectic mesophases.[10] Add a few lines about applications? We show first that our MD simulation results for the morphology are consistent with wide angle X-ray scattering data and predict a phase transition from smectic to the isotropic phase in fair agreement with experiment.[10] We then demonstrate that in a system with reduced energetic disorder, the decrease in orientational order with increasing temperature does not affect the magnitude of the diffusion length L_d. We also find, however, that the directionality of the exciton dynamics is affected resulting in a loss of the transport anisotropy at high temperatures. These results help to build an understanding of how morphology and chemical structure synergistically influence exciton transport, which is an essential prerequisite in order to fully exploit the potential applications of organic devices.

Computational Details

Molecular Dynamics simulations

Molecular Dynamics simulations of bulk IF3 samples in the NPT ensemble were conducted with the NAMD code,[11] integrating the equations of motion with a time step of 2 fs for short range and bonded interactions, and 4 fs for long range non bonded interactions. Both pressure and temperature were controlled with weak coupling schemes.[12] We adopted the CHARMM potential

energy function,[13] composed of harmonic stretching and bending terms, dihedrals described by a series of cosines, and Coulomb and Lennard-Jones terms for non-bonded interactions. Electrostatic interactions were calculated with the PME method with a mesh spacing of about 1.5 Å,[14] whilst a cutoff of 10 Å was employed in the evaluation of Lennard-Jones terms. IF3 molecules were described at united atom (UA) level, i.e., without explicit hydrogens. This approach offers the advantage of reducing the number of centers while retaining a good accuracy of the static physical properties;[15–17] the dynamics instead can be faster than experiment,[16,18] but this side-effect is not necessarily a drawback as it improves the phase sampling and thus reduces the equilibration times.

Both atomic charges at the equilibrium geometry and the torsional potential for the angle ϕ between two indenofluorene monomers were calculated with the DFT method as implemented in the Turbomole 5.9 code,[19] using the 6-31G basis set and the B3LYP functional. In all these calculations octyl chains were omitted and replaced by hydrogens. To comply with the UA model, at each UA center was assigned the sum of the charges of the corresponding carbon and its geminal hydrogens, and charges on chemically equivalent centers were equalized; alkyl chain charges were instead zeroed like in Ref.[17] In order to reproduce the *ab initio* torsional potential with the classical force field we used the approach described in Ref.[20] to take into account the non-bonded interaction contributions. Aromatic carbons without implicit hydrogens and aliphatic carbons were described with the AMBER UA force field,[21,22] while aromatic carbons with one implicit hydrogen were parameterized following Ref.[23]

A low density ($\approx$0.1 g/cm^3) sample of 128 IF3 molecules parallely arranged was built and quickly compressed applying a pressure of 1000 atm at 400 K until obtaining a density of about 1 g/cm^3, a box size of about 90 x 80 x 60 Å , a smectic order parameter $\tau = 0.4$, a nematic order parameter $P_2 = 0.76$ with the director oriented along the z axis. This configuration was used as starting geometry for simulation runs at 350, 375, 400, 425, 450, 475, 500 K and pressure of 1 atm. At the three higher temperatures the order parameter dropped to isotropic values after 20-40 ns and the runs were not proceeded further. For the other temperatures we performed equilibration runs of 100 ns, during which P_2 reached a stationary value after an initial decrease, with the exception

of T=425 K which exhibited a continuous slow decay. After this preliminary step, the boxes were doubled along the z axis and the new 256-molecule samples were simulated at the same temperatures and pressure. Two additional temperatures, 300 and 325 K were started from the 350 K configuration. These large samples were further equilibrated until reaching constant density and P_2; this required from 80 to 300 ns of simulation. Finally, production runs were performed, with duration decreasing with temperature, ranging from 170 ns at 300 K to 60 ns at 500 K; during the runs, configurations were stored with a frequency of 100 ps and afterwards processed for calculating the observables reported in this work.

Quantum-Chemical calculations and Monte Carlo energy transport simulations

In the weak coupling regime appropriate here (vide infra), excitons are localised on single molecular sites and exciton transfer takes place via resonant energy transfer from a donor molecule D in the excited state to an acceptor molecule A in its ground state.[24] The rate of hopping can be expressed as:[25,26]

$$k_{DA} = \frac{2\pi}{\hbar}|V_{DA}|^2 J_{DA} \,, \tag{1}$$

with V_{DA} the excitonic coupling and J_{DA} the spectral overlap between the donor emission $F_D(\omega)$ and the acceptor absorption spectra $A_A(\omega)$, given by:

$$J_{DA} = \int_0^\infty F_D(\omega) A_A(\omega) d\omega \,. \tag{2}$$

We have calculated the excitonic coupling between all donor D molecules and each of the fifty nearest neighbor acceptor A oligomers using the distributed monopole approximation[27–30] that expresses V_{DA} as a Coulomb interaction term:

$$V_{DA} = \frac{1}{4\pi\varepsilon_0} \sum_{i\in D} \sum_{j\in A} \frac{\rho_D(\vec{r}_{D_i})\rho_A(\vec{r}_{A_j})}{|\vec{r}_{D_i} - \vec{r}_{A_j}|} \,, \tag{3}$$

where the sum runs over the donor $\vec{r}_{D_i}$ and acceptor $\vec{r}_{A_j}$ atomic positions produced by the MD simulation, ρ are the atomic transition charge densities and ε_0 the vacuum permittivity. The transition charges have been computed through correlated coupled cluster calculations,[31] using the intermediate neglect of differential overlap INDO Hamiltonian.[32] This was done for all 256 chromophores in the sample for representative configurations of the morphology at each temperature.

The absorption and emission spectra of indenofluorene trimers at different temperatures have been obtained by means of *ab initio* simulations. In more detail, we have calculated the equilibrium ground and first excited state geometries and frequencies at the DFT and TD-DFT levels, respectively. The geometric distortions between the ground and excited state geometries were mapped onto the ground and excited state normal modes in the case of the absorption and emission spectra, respectively. In contrast to previous studies where only a few effective modes were considered, here all vibrational modes, but librations, have been used in an undistorted displaced harmonic oscillator model. The librational modes, that give rise to large distortions when going from the ground state to the excited state, have been treated as in reference.[33] Anharmonic effects are taken into account by numerical diagonalization of the nuclear Hamiltonian obtained from the (TD-)DFT calculations. This model leads to a natural description of the mirror asymmetry between the absorption and emission spectra as well as of the Stokes shift. The lineshape is not treated here as an adjustable parameter but is the direct result of the thermal population of (mostly) the soft libration modes.[33] As will be shown below each molecule explores locally the torsion potential energy surface over time scales that are short compared to the exciton hopping time, contributing thereby to the dynamic homogeneous linewidth. Large amplitude conformational changes (involving crossing the barrier at 90°, 0° and 180°) occur on much longer times and yield a distribution of conformers that can safely be assumed to be static in nature during the exciton lifetime?. Another contribution to energetic disorder arises from the dielectric environment and can be introduced through a random rigid shift of absorption and emission spectra, as extracted from a Gaussian distribution of width σ.

We use kinetic Monte Carlo simulations to model the exciton diffusion as a random walk of discrete steps in space. The model requires as an input the molecular positions, provided by the MD simulations and the exciton transfer rates between molecular sites, calculated at the quantum-chemical level. An exciton is randomly placed in the system and a waiting time to hop from oligomer i to a neighboring oligomer j is sampled from an exponential distribution:[34,35]

$$\tau_{ij} = -\frac{1}{k_{ij}} \ln X \ , \tag{4}$$

where k_{ij} is the transfer rate between i and j and X is a random number between 0 and 1. Additionally, in competition with the transfer?, a recombination time is calculated as $\tau_i^R = -\tau_L \ln X$, with τ_L the radiative lifetime of an excitation localised on an indenofluorene trimer and calculated to be 655 ps.[36] On each MC step the event demanding the smallest waiting time is selected and executed until the exciton eventually recombines. Quantities of interest are sampled from a large number of exciton trajectories (exciton trials) of the order of 10^6 and the exciton diffusion length is obtained by averaging the individual diffusion lengths of all trials, $L_d^{trial} = \sqrt{\Delta x^2 + \Delta y^2 + \Delta z^2}$, where Δx, Δy and Δz are the x, y, z components of the displacement between the initial and final point on the exciton trajectory, calculated without imposing 3D boundary conditions. This procedure gives a variance of 0.2 nm on L_d of each MD configuration. The final diffusion length $\langle L_d \rangle$ is extracted as the ensemble average performed on all snapshots of given temperature.

Results and Discussion

Phase behaviour of indenofluorene trimers

In this section we describe the temperature dependence of the bulk phase physical properties of IF3 as obtained from MD simulations. The purpose of the investigation is twofold: on one hand, to assess the microscopic structure of the material and validate it through the comparison with experimental data, on the other to obtain atomic coordinates which are necessary for a realistic

simulation of the energy transport process in the system. Similarly to the corresponding polymer 2,8-poly-6,6′,12,12′-tetraoctyl-6,12-dihydroindeno [1,2*b*] fluorene,[37] IF trimers are known to form a liquid crystalline phase above their glass transition temperature (that occurs at 261 K), namely a smectic phase which melts at 411 K.[10] The reproduction of this phase transition and of the temperature it occurs with atomistic simulations is challenging[38,39] but in this case necessary to prove the reliability of the simulation results.

Starting from an ordered sample, the onset of the disordering transition was monitored through the average values of the nematic order parameter $\langle P_2 \rangle = \langle 3(\mathbf{u} \cdot \mathbf{n})^2 - 1 \rangle / 2$, which reflects the orientational order of the long molecular axis **u**, calculated as the unit vector joining the aromatic carbons at the two ends of IF3, with respect to the phase director **n** (see ref.[16] for details).

In Figure 1 we report the ensemble average of P_2 at each temperature, which shows a smooth and progressive decrease of the orientational order when increasing T, until isotropization occurs above 400 K. To characterize the nature of the mesophases it is also useful to monitor the extent of positional order along the alignment direction $\mathbf{z} \parallel \mathbf{n}$ through the smectic order parameters $\langle \tau_n \rangle$. We measured them by a least square fitting of the scaled density function along **z** with the first four terms of the following expression due to McMillan:[40]

$$\rho(z)/\rho_0 = 1 + \langle \tau_1 \rangle \cos(2\pi z/\langle d \rangle) + \ldots + \langle \tau_n \rangle \cos(n 2\pi z/\langle d \rangle). \quad (5)$$

This method allows to derive the layer spacing $\langle d \rangle$ of the smectic phase, which yields a constant value of $\langle d \rangle = 31.5$ Å, corresponding approximately to the end-to-end distance of the trimer. The temperature dependence of the order parameter $\langle \tau_1 \rangle$ resulting from the fitting procedure is reported in Figure 1, clearly showing the presence of a smectic phase at temperatures below 400 K; the higher terms $\langle \tau_2 \rangle$ and $\langle \tau_3 \rangle$ were found to be rather small (< 0.01) but following the same behaviour of $\langle \tau_1 \rangle$. The periodicity of the density fluctuations along **z**, typical of the smectic phase, and the applicability of equation 5 can be better appreciated in Figure 2, where the normalized density at 300 K is plotted against its fitting function. The snapshot on the top reveals the corresponding

molecular arrangement, typical of a smectic A phase, in which the molecular centers of masses are distributed on diffuse layers perpendicular to the ordering direction (indicated with vertical orange bars), with liquid-like positional disorder within the layers.

To confirm the presence of a phase transition and to better characterize it, we investigated the overall and internal rotational dynamics of the systems through the autocorrelation functions $C_f(t) = \langle f(0) \cdot f(t) \rangle$, where f can be either **u** (short or long molecular axes), or the sine of dihedral angle ϕ between linked monomers (cf. Figure 3). The intrisic decay times for the property $f(t)$can in principle be calculated by integrating $C_f(t)$:[41]

$$\tau^f_{rot} = \int_0^\infty \frac{C_f(t) - C_f(\infty)}{C_f(0) - C_f(\infty)} dt \tag{6}$$

To account for the fact that the decay times of these functions can be much longer than the simulation time, as the rotation is progressively hindered by lowering the temperature, we extrapolated the long-time behaviour by fitting their short time profile (first half of the trajectory) with a sum of three exponentials. This functional form presents the benefit of not making assumptions on the symmetry of the rotational diffusion tensor.[42] We then estimated the rotational decay time from equation 6 replacing $C(t)$ with its fitting function. The procedure, albeit somewhat arbitrary, allows to clearly identify the temperature trends of the rotational times, which are shown in Figure 3, where two separate regions with different activation energy are clearly visible, at low T (corresponding to the smectic phase), and at high T (isotropic phase). The relaxation times in the smectic phase appear to be much higher than the simulated time window (hence subjected to a large uncertainity), revealing that the rotational motion in this phase is severely hindered and hinting to a high viscosity, All these indicators confirm a phase transition between 375 and 400 K; the same conclusion holds for the temperature behaviour of the translational diffusion coefficient (see Figure SI 3).

Once assessed that the simulations reproduce the experimental phases and thermal behaviour with reasonable accuracy, it is worth analyzing some details of the molecular arrangement of IF3 in

the condensed phase. In particular it is interesting to monitor the conformation of the intermonomer dihedral ϕ, which can influence the photoluminescence of these materials through promoting or preventing the intermolecular aggregation.[43]

Similarly to what has been observed and calculated for oligofluorenes,[44–46] for oligophenyls in gas phase,[47,48] and for biphenyls dissolved in liquid crystals,[49] the ground state is not planar and presents here an average value of the torsional angle ϕ of $\pm$ 38°+kπ, both in the smectic and in the isotropic phase of IF3. In our case the peaks of the distribution of ϕ can be well interpolated with gaussian functions; their standard deviation increases linearly with temperature from 9° to 13°, but does not show significant changes at the smectic-isotropic transition. As mentioned above, the torsion angles vary quickly (compared to the exciton hopping time) around the equilibrium ground-state values, Figure 5, so that coupling to intramolecular vibrational modes can be described as homogeneous; on the contrary conformational jumps are much slower and result in decay times that span a large time domain, from ∼0.5 ns at 500 K to ∼300 ns at 300 K, Figure 3.

The packing of the molecules in the smectic phase can be appreciated by inspecting the radial distribution function (rdf, not shown) of the different atom types composing the molecule. Along the meridional direction (parallel to **n**) all aromatic carbon rdfs are dominated by the monomer-monomer repeating distance of 12.5 Å, in perfect agreement with the analysis of the polymer X-ray spectrum (12.5 Å[50]); the small difference with the position of the intense meridional reflection registered for the trimer (d_{me}=11.7 Å[10]) can be explained with the fact that the molecules are slightly bent, so even if two linked monomers are 12.5 Å apart, the third closest monomer is separated by only 23.5 Å from the first, and finally the closest fourth monomer (belonging to another molecule) is 31.5 Å apart, which is indeed the layer spacing of the smectic phase (cf Figure 2). We therefore suggest that the peak at 11.7 Å contains the contribution of all these reflections.

In the equatorial direction (perpendicular to **n**) the most important distance is the separation between the first neighbor for molecules belonging to the same smectic layer (d_{eq}=8.5 Å vs 8.8 Å reported in[10]), together with the distance of the second neighbour (16.1 Å); in addition a shoul-

der centered at around 14.7 Å ($=\sqrt{3}d_{eq}$) reveals the presence of non negligible hexagonal order inside the layer. Finally, it is remarkable to stress the lack of evidence for π stacking and herringbone packing both in simulation morphologies and in the WAXS patterns: the octyl substituents seem to prevent these arrangements, typical of planar aromatic compounds, favoring instead the isolation of the aromatic backbones, which are immersed in a bath of entangled alkyl chains. This organization is also expected to yield excitons that are confined on single IF3 units rather than being delocalized over molecular aggregates.

Energy transport in the condensed phase

The simulation of the energy transport process relies on the correct prediction of the absorption and emission spectra. The calculated spectra at 300 K are displayed in Figure 6 along with the experimental spectra in solution and film.[10] We observe an overall good agreement on the shape, linewidth and Stokes shift (≈ 0.26 eV); the absorption spectrum consists of a featureless broad peak while emission exhibits a clear vibronic structure. This loss of mirror symmetry as well as the relative intensity of the emission peaks are reproduced by our *ab initio* calculations discussed earlier. We should emphasize that this agreement is established without any fitting procedure; the only adjustment was a blue-shift of the simulated spectra by 7 nm to match the exact positions of the absorption and first emission peaks to the experimental ones. The similar vibronic progression of the IF3 experimental photoluminescence spectra in film and solution, and the fact that the absorption features hardly change when going from solution to the LC phase, as demonstrated for similar indenofluorene trimers[44] and for the polymer[51], indicates that the weak intermolecular coupling regime is a reasonable assumption for our model. Note that the reduced intensity of the 0-0 line in the photoluminescence spectrum of the film is mostly due to self-absorption effects.[10]

To further validate the choice of the appropriate transport regime we have calculated the maximum excitonic coupling between first nearest neighbors averaged on all different configurations, $\langle |V_{DA}^{max}| \rangle = 0.0379$ eV at 300 K, found to be much smaller than the value of the excited state reorganization energy, $\lambda = 0.34$ eV at 300 K,[33] ensuring that transport occurs via incoherent hopping

of excitons localized on single IF3 chromophores.

The spatial extent over which an excitation could diffuse during its lifetime depends on the rate of energy transfer which in turn is proportional to the squared excitonic coupling $|V_{DA}|^2$ and the spectral overlap via eq. 1. As a prelude to the full transport simulations, we explore how sensitive V_{DA} is to changes on the molecular conformations. The square of the excitonic coupling for two molecules of IF3 is sensitive to the rigid body rotation angle θ about the axis connecting the centre of masses of the two molecules; in more detail, $|V_{DA}|^2$ is an oscillating function of θ with a period of π, reflecting the fact that the excitonic coupling is maximized when the transition dipoles are parallel to each other, $\theta = 0^\circ$, and vanishes for perpendicular orientation of the dipoles, $\theta = 90^\circ$ (see Figure SI 4). From these considerations it is expected that the coupling will globally decrease with increasing orientational and positional disorder (following from the increase in temperature) since there will be an increasing probability of finding neighboring chromophores misaligned. The electronic structure calculations confirm this scenario as can be seen on Figure 7 and from the probability distribution plot of $|V_{DA}|^2$ for the smectic phase at 300 K and the isotropic phase at 500 K (see Figure SI 5). However, one has to take into account that the spectral overlap is also sensitive to temperature changes and in particular its value is increased with temperature due to the broadening of the spectra. In Figure 7 we see that J_{DA} calculated from the simulated oligomer absorption and emission spectra increases linearly with T. Overall, the combined effect of reduced electronic coupling and increased spectral overlap thus results in a constant total hopping rate (the ensemble average of the sum of all possible hopping rates for each molecule), as can be seen on the inset of Figure 8.

Having examined the sensitivity of the microscopic parameters that control energy transport we now turn our attention to the Monte Carlo simulations of exciton diffusion. We find that L_d is almost independent of temperature with a mean value of 67.5 nm, as depicted in Figure 8. It is at first surprising that for all studied morphologies the diffusion length is constant as it would be tempting to assume that L_d should be smaller for the more disordered morphologies. Nevertheless, as demonstrated above, although on average $|V_{DA}|^2$ reduces with increasing temperature, it is com-

pensated by the increase in J_{DA}, resulting in a constant transfer rate and henceforth diffusion length. It is therefore the combined effect of reduction in $|V_{DA}|^2$ and increase in J_{DA} that leads to a constant L_d. We should also emphasize that it has been generally believed that the singlet exciton diffusion length in amorphous organic materials should be very small.[7,52,53] In contrast, our simulations suggest that the above dogma is not necessarily true and large values of L_d could be expected even in disordered organic materials. To provide a magnitude for a measurable quantity, we have also extracted an effective, orientation averaged, Förster radius (the distance at which $\langle k_{DA} \rangle = 1/\tau^R$). Our calculated value of 3.23 nm at 300 K is close to the experimentally determined value of ≈ 3.3 nm (probably at ambient temperature, not specified explicitly in their paper though) obtained from photoluminescence experiments in samples of perylene end-capped polyindenofluorene chains.[54] It is interesting to note that the calculated Förster radius also follows the same trend of L_d, being nearly independent of temperature.

However, the reduction of the order parameters (Figure 1) plays an important role on the diffusion and the pathways that excitons follow. Indeed, as we observe on Figure 8, excitons do benefit from orientational order and better packing, travelling larger distances at the direction perpendicular to the smectic layers (z-direction, Figure 2 top panel) at lower temperatures. The anisotropy of energy transfer in liquid crystals has been predicted in the past by molecular level simulations;[55,56] the knowledge this property, which is very sensitive to the aspect ratio and intermolecular distances between chromophoric units,[55,57] could in principle be exploited in designinig favorable pathways for excitions in devices REMOVE IF YOU DON'T LIKE. As temperature increases transport eventually becomes isotropic via the transition to the isotropic phase: the impact of temperature on the diffusion dynamics can hence be related to the different pathways excitons use to diffuse while overall the diffusion length remains unaltered.

Another physical property that can be easily accessed by fluorescence spectroscopy, and in this case by simulations, is the anisotropy ratio as a function of time $r(t) = (I_{\parallel} - I_{\perp})/(I_{\parallel} + 2I_{\perp})$. Here we suppose to excite at $t = 0$ our sample with vertically (parallel to $\mathbf{n}$) polarised light and to measure the intensity of light exiting the sample either in the parallel ($I_{\parallel}$) or perpendicular direction

($I_\perp$) at a given time. As the transition dipoles μ for IF3 are parallel to the long molecular axis **u**, we computed the two relative intensities as:[58]

$$I_\parallel = \langle u_z(0)^2 u_z(t)\rangle \exp(t/\tau_L) \quad (7)$$

$$I_\perp = 0.5\,(\langle u_z(0)^2 u_x(t)^2\rangle + \langle u_z(0)^2 u_y(t)^2\rangle)\exp(t/\tau_L). \quad (8)$$

The fluorescence anisotropy, plotted in Figure 9, is clearly temperature dependent as it is reminiscent of the average orientational order through its asymptotic value $r(\infty) = \langle P_2\rangle$, allowing to distinguish the smectic phase (T=300, 350 and 400 K in Figure 9) from the isotropic phase (T=450 and 500 K), where the long-time emission is completely depolarised ($r = 0$). At short times instead the anisotropy is always higher as the the incident light is parallelly polarised, but it quickly reaches the asymptotic behavior in about 5 ps at all temperatures, with lifetimes, obtained with equation 6, ranging from 0.2 to 0.3 ps. These times are of the same order of magnitude of the average exciton waiting times (Figure SI 6), revealing that in practice only a few exciton hops are sufficient to reach the steady state anisotropy.

Finally, we explore the role of static energetic disorder on exciton diffusion. As discussed before, conformational disorder (arising from local fluctuations of the torsion angles between the indenofluorene units) is dynamic and accounted for explicitly in the homogeneous linewidth. An additional contribution to the spectral lineshapes usually arises when embedding molecules in a dielectric environment and is included in transport models through a random distribution of site energies obeying Gaussian distribution of width σ. To give a flavour on the effects of inhomogeneous disorder, we show in Figure 10 the calculated diffusion length as a function of σ. We note that L_d decreases when σ increases, as documented in previous works.[9] Furthermore, this decrease is steeper for the lowest temperatures since there is less thermal energy available to overcome energy barriers. Therefore, high values of static disorder could lead to a different behavior making L_d sensitive to temperature. However, as an inhomogeneous broadening of only 0.014 eV

has been reported for a similar step ladder type paraphenylene oligomer,[59] energetic disorder is expected to be low in our system. To quantify the magnitude of electrostatic disorder associated with molecules feeling different dielectric environment, we have calculated the distribution of the difference between the ground and excited state electrostatic energy of the IF3 molecules. The distributions (see Supporting Information Figure SI 7) were fitted reasonably well with Gaussian functions and possess standard deviations lower than 0.007 eV: it is clear from Figure 10 that such low values of disorder play a marginal role on the temperature dependence of the exciton diffusion length.

Conclusions

We have presented a detailed atomistic study of exciton transport in conjugated oligomers by combining MD, quantum chemistry and MC simulations. The validity of the MD simulation results is supported by recent experimental data on indenofluorene mesophases. We demonstrate that, unexpectedly, the diffusion length is not affected by the reduction of the order parameters with increasing temperature. This is attributed to the cancelling effect of the global decrease of the average excitonic coupling and the simultaneous increase of the spectral overlap with increasing temperature. Whilst the phase transition from smectic to isotropic phase does not impact the magnitude of L_d, it has a remarkable effect on the directionality of the exciton transport, which is anisotropic at room temperature (in the smectic phase) and reaches purely isotropic behaviour only at high temperatures. Our approach adds realism to modelling the transport properties of conjugated systems and sheds light on the impact of both the morphological and temperature change in the material to its optoelectronic properties and therefore the device characteristics. The above results suggest that liquid crystalline oligomeric materials could be promising candidates for engineering optoelectronic devices that require stable and controlled electronic properties over a wide range of temperatures and supramolecular arrangements.

Acknowledgement

The authors would like to thank Dr. Johannes Gierschner (IMDEA Madrid) for helpful discussions. The research leading to these results has received funding from the European Community through FP6 project MODECOM (NMP-CT-2006-016434) and FP7 project ONE-P (NMP3-LA-2008-212311). S. A. and D. B. are respectively Postdoctoral Research Fellow and Research Director at FNRS.

References

(1) Burroughes, J. H.; Bradley, D. D. C.; Brown, A. R.; Marks, R. N.; Mackay, K.; Friend, R. H.; Burns, P. L.; Holmes, A. B. *Nature* **1990**, *347*, 539.

(2) Sirringhaus, H.; Brown, P. J.; Friend, R. H.; Nielsen, M. M.; Bechgaard, K.; Langeveld-Voss, B. M. W.; Spiering, A. J. H.; Janssen, R. A. J.; Meijer, E. W.; Herwig, P.; de Leeuw, D. M. *Nature* **1999**, *401*, 685.

(3) III, S. T.; Joly, G.; Swager, T. *Chem. Rev.* **2007**, *107*, 1339.

(4) Li, G.; Shrotriya, V.; Huang, J. S.; Yao, Y.; Moriarty, T.; Emery, K.; Yang, Y. *Nat. Mater.* **2005**, *4*, 864.

(5) Peumans, P.; Yakimov, A.; Forrest, S. R. *J. Appl. Phys.* **2003**, *93*, 3693.

(6) Campoy-Quiles, M.; Ferenczi, T.; Agostinelli, T.; Etchegoin, P. G.; Kim, Y.; Anthopoulos, T. D.; Stavrinou, P. N.; Bradley, D. D. C.; Nelson, J. *Nat. Mater.* **2008**, *7*, 158.

(7) Blom, P. W. M.; Mihailetchi, V. D.; Koster, L. J. A.; Markov, D. E. *Adv. Mater.* **2007**, *19*, 1551.

(8) Müllen, K.; Wegner, G. *Electronic materials: The Oligomer approach*; Wiley-VCH Weinheim, 1998.

(9) Athanasopoulos, S.; Emelianova, E. V.; Walker, A. B.; Beljonne, D. *Phys. Rev. B* **2009**, 195209.

(10) Elmahdy, M. M.; Floudas, G.; Oldridge, L.; Grimsdale, A. C.; Müllen, K. *ChemPhysChem* **2006**, *7*, 1431–1441.

(11) Phillips, J. C.; Braun, R.; Wang, W.; Gumbart, J.; Tajkhorshid, E.; Villa, E.; Chipot, C.; Skeel, R. D.; Kale, L.; Schulten, K. *J. Comput. Chem.* **2005**, *26*, 1781–1802.

(12) Berendsen, H. J. C.; Postma, J. P. M.; Nola, A. D.; Haak, J. R. *J. Chem. Phys.* **1984**, *81*, 3684–3690.

(13) MacKerell, A. D. et al. *J. Phys. Chem. B* **1998**, *102*, 3586–3616.

(14) Essmann, U.; Perera, L.; Berkowitz, M. L.; Darden, T. A.; Lee, H.; Pedersen, L. G. *J. Chem. Phys.* **1995**, *101*, 8577–8593.

(15) Marcon, V.; Vehoff, T.; Kirkpatrick, J.; Jeong, C.; Yoon, D. Y.; Kremer, K.; Andrienko, D. *J. Chem. Phys.* **2008**, *129*, 094505.

(16) Tiberio, G.; Muccioli, L.; Berardi, R.; Zannoni, C. *ChemPhysChem* **2009**, *10*, 125–136.

(17) Olivier, Y.; Muccioli, L.; Lemaur, V.; Geerts, Y. H.; Zannoni, C.; Cornil, J. *J. Phys. Chem. B* **2009**, *113*, 14102–14111.

(18) Budzien, J.; Raphael, C.; Ediger, M. D.; de Pablo, J. J. *J. Chem. Phys.* **2002**, *116*, 8209–8217.

(19) Furche, F.; Ahlrichs, R. *J. Chem. Phys.* **2002**, *117*, 7433–7447.

(20) Berardi, R.; Cainelli, G.; Galletti, P.; Giacomini, D.; Gualandi, A.; Muccioli, L.; Zannoni, C. *J. Am. Chem. Soc.* **2005**, *127*, 10699–10706.

(21) Cornell, W. D.; Cieplak, P.; Bayly, C. I.; Gould, I. R.; Merz Jr., K. M.; Ferguson, D. M.; Spellmeyer, D. C.; Fox, T.; Caldwell, J. W.; Kollman, P. A. *J. Am. Chem. Soc.* **1995**, *117*, 5179.

(22) Yang, L. J.; Tan, C. H.; Hsieh, M. J.; Wang, J. M.; Duan, Y.; Cieplak, P.; Caldwell, J.; Kollman, P. A.; Luo, R. *J. Phys. Chem. B* **2006**, *110*, 13166–13176.

(23) von Lilienfeld, O. A.; Andrienko, D. *J. Chem. Phys.* **2006**, *124*, 054307.

(24) May, V.; Kühn, O. *Charge and Energy Transfer Dynamics in Molecular Systems*; Wiley-VCH, Berlin, 2000.

(25) Hennebicq, E.; Beljonne, D.; Curutchet, C.; Scholes, G. D.; Silbey, R. J. *J. Chem. Phys.* **2009**, *130*, 214505.

(26) Beljonne, D.; Curutchet, C.; Scholes, G. D.; Silbey, R. J. *J. Phys. Chem. B* **2009**, *113*, 6583–6599.

(27) Marguet, S.; Markovitsi, D.; Millié, P.; Sigal, H.; Kumar, S. *J. Phys. Chem. B* **1998**, *102*, 4697–4710.

(28) Beljonne, D.; Cornil, J.; Silbey, R.; Millié, P.; Brédas, J.-L. *J. Chem. Phys.* **2000**, *112*, 4749–4758.

(29) Hennebicq, E.; Pourtois, G.; Scholes, G.; Herz, L.; Russell, D.; Silva, C.; Setayesh, S.; Grimsdale, A.; Müllen, K.; Brédas, J.-L.; Beljonne, D. *J. Am. Chem. Soc.* **2005**, *127*, 4744–4762.

(30) Bacchiocchi, C.; Hennebicq, E.; Orlandi, S.; Muccioli, L.; Beljonne, D.; Zannoni, C. *J. Phys. Chem. B* **2008**, *112*, 1752–1760.

(31) Shuai, Z.; Brédas, J. L. *Phys. Rev. B* **2000**, *62*, 15452.

(32) Ridley, J.; Zerner, M. C. *Theor. Chim. Acta* **1973**, *32*, 111–134.

(33) Heimel, G.; Daghofer, M.; Gierschner, J.; List, E. J. W.; Grimsdale, A. C.; Beljonne, D.; Bredas, J. *J. Chem. Phys.* **2005**, *122*, 054501.

(34) Jansen, A. P. J. *Comp. Phys. Comm.* **1995**, *86*, 1.

(35) Lukkien, J. J.; Segers, J. P. L.; Hilbers, P. A. J.; Gelten, R. J.; Jansen, A. P. J. *Phys. Rev. E* **1998**, *58*, 2598.

(36) Athanasopoulos, S.; Hennebicq, E.; Beljonne, D.; Walker, A. B. *J. Phys. Chem. C* **2008**, *112*, 11532–11538.

(37) Setayesh, S.; Marsitzky, D.; Müllen, K. *Macromolecules* **2000**, *33*, 2016–2020.

(38) Cacelli, I.; De Gaetani, L.; Prampolini, G.; Tani, A. *J. Phys. Chem. B* **2007**, *111*, 2130–2137.

(39) Böckmann, M.; Peter, C.; Delle Site, L.; Doltsinis, N. L.; Kremer, K.; Marx, D. *J. Chem. Theory Comput.* **2007**, *3*, 1789–1802.

(40) McMillan, W. L. *Phys. Rev. A* **1972**, *6*, 936–947.

(41) Zannoni, C. In *The Molecular Dynamics of Liquid Crystals*; Luckhurst, G., Veracini, C., Eds.; Kluwer, 1994; Chapter 6, pp 139–169.

(42) Wong, V.; Case, D. A. *J. Phys. Chem. B* **2008**, *112*, 6013–6024.

(43) Lim, S.-F.; Friend, R. H.; Rees, I. D.; Li, J.; Ma, Y.; Robinson, K.; Holmes, A. B.; Hennebicq, E.; Beljonne, D.; Cacialli, F. *Adv. Funct. Mater.* **2005**, *15*, 981–988.

(44) Chi, C.; Lieser, G.; Enkelmann, V.; Wegner, G. *Macromol. Chem. Phys.* **2005**, *206*, 1597–1609.

(45) Marcon, V.; van der Vegt, N.; Wegner, G.; Raos, G. *J. Phys. Chem. B* **2006**, *110*, 5253–5261.

(46) Kilina, S.; Batista, E. R.; Yang, P.; Tretiak, S.; Saxena, A.; Martin, R. L.; ; Smith, D. L. *ACS Nano* **2008**, *2*, 1381–1388.

(47) Cacelli, I.; Prampolini, G. *J. Phys. Chem. A* **2003**, *107*, 8665–8670.

(48) Lukeš, V.; Šolc, R.; Barbatti, M.; Elstner, M.; Lischka, H.; Kauffmann, H.-F. *J. Chem. Phys.* **2008**, *129*, 164905.

(49) Catalano, D.; Di Bari, L.; Veracini, C. A.; Shilstone, G. N.; Zannoni, C. *J. Chem. Phys.* **1991**, *94*, 3928–3935.

(50) Keivanidis, P. E.; Jacob, J.; Oldridge, L.; Sonar, P.; Carbonnier, B.; Baluschev, S.; Grimsdale, A. C.; Müllen, K.; Wegner, G. *ChemPhysChem* **2005**, *6*, 1650–1660.

(51) Ye, J.; Grimsdale, A. C.; Zhao, Y. *J. Phys. Chem. A* **2010**, *114*, 504–508.

(52) Mikhnenko, V.; Cordella, F.; Sieval, A. B.; Hummelen, J. C.; Blom, P. W. M.; Loi, M. A. *J. Phys. Chem. B* **2008**, *112*, 11601.

(53) Shaw, P. E.; Ruseckas, A.; Samuel, I. D. W. *Adv. Mater.* **2008**, *20*, 3516.

(54) Herz, L. M.; Silva, C.; Grimsdale, A. C.; Müllen, K.; Phillips, R. T. *Phys. Rev. B* **2004**, *70*, 165207.

(55) Bacchiocchi, C.; Zannoni, C. *Chem. Phys. Lett.* **1997**, *268*, 541–548.

(56) Bacchiocchi, C.; Zannoni, C. *Phys. Rev. E* **1998**, *58*, 3237–3244.

(57) Gierschner, J.; Huang, Y.-S.; Van Averbeke, B.; Cornil, J.; Friend, R. H.; Beljonne, D. *J. Chem. Phys.* **2009**, *130*, 044105.

(58) Zannoni, C. *Mol. Phys.* **1979**, *38*, 1813–1827.

(59) Wiesenhofer, H.; Zojer, E.; List, E. J. W.; Scherf, U.; Brédas, J. L.; Beljonne, D. *Adv. Funct. Mater.* **2006**, *18*, 310.

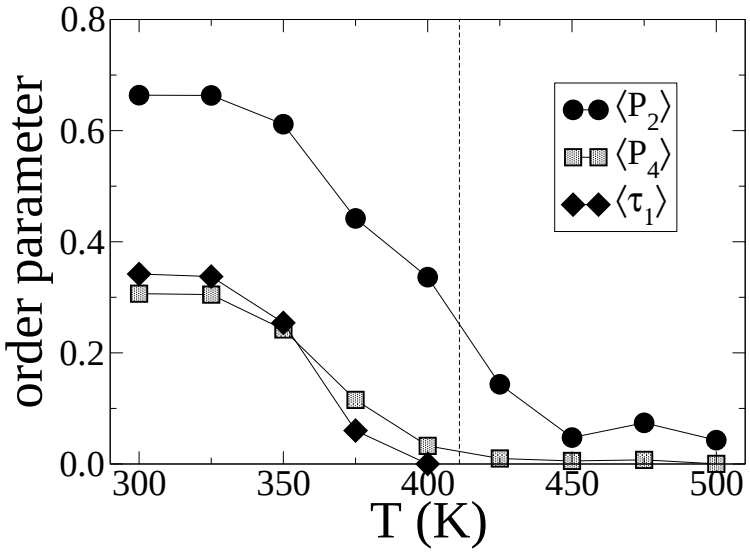

Figure 1: Temperature dependence of order parameters: average nematic second and fourth order parameters $\langle P_2 \rangle$, $\langle P_4 \rangle$ and average smectic order parameter $\langle \tau_1 \rangle$

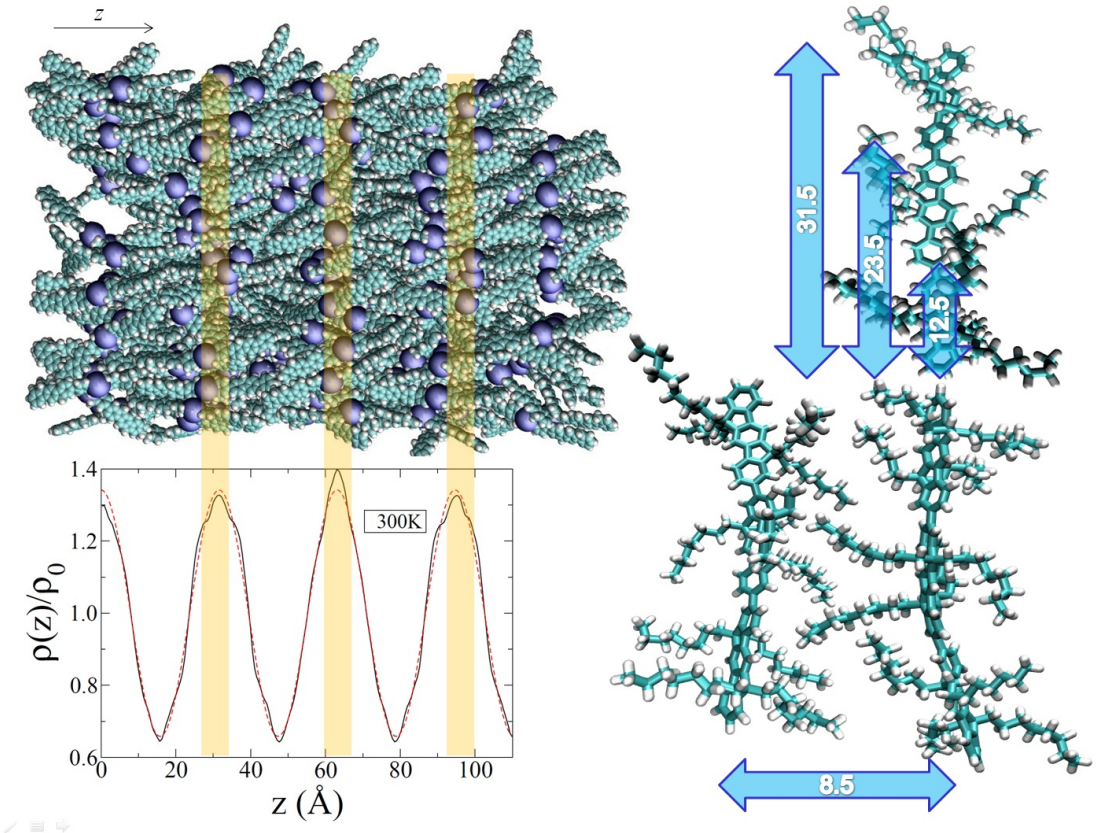

Figure 2: Top left panel: A snapshot of 256 IF3 molecules in the smectic phase at 300 K (top, alkyl chains omitted for clarity, hydrogen atoms artificially added, blueish spheres indicate IF3 centers of mass). Bottom left panel: The scaled density distribution function along the alignment direction z (red line). Orange vertical bars underline the correspondence of the peaks of the density distribution with the layers in the snapshot. Right panel: A schematization of the most representative intermonomer distances in the smectic phase (units in Å).

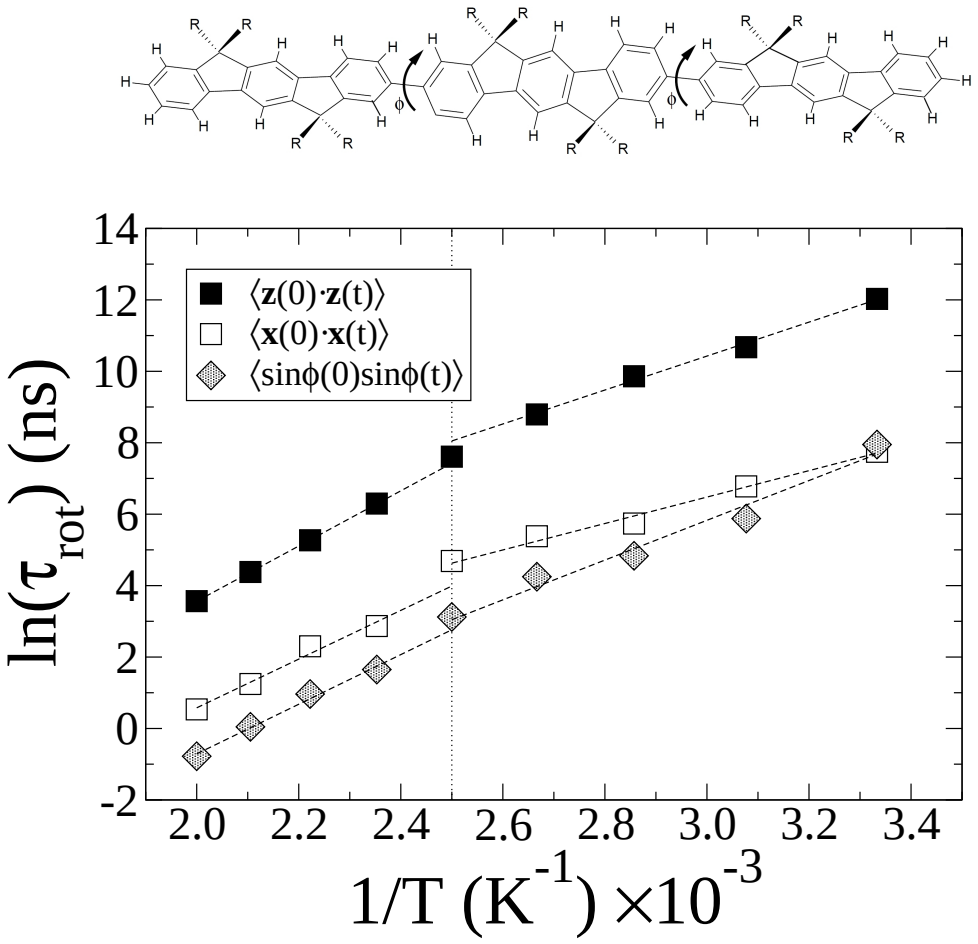

Figure 3: Top panel: Chemical sketch of the 6,6′,12,12′-tetraoctylindenofluorene trimer studied in this work (R= n-octyl chains), with monomer-monomer dihedral angles indicated.
Bottom panel: Arrhenius plot of some rotational diffusion indicators: decay times of the autocorrelation function of the molecular axes **z** (black squares) and **x** (white squares), and of the sine of the dihedral angle ϕ (grey rhombs). All indicators suggest a phase transition between 375 and 400 K.

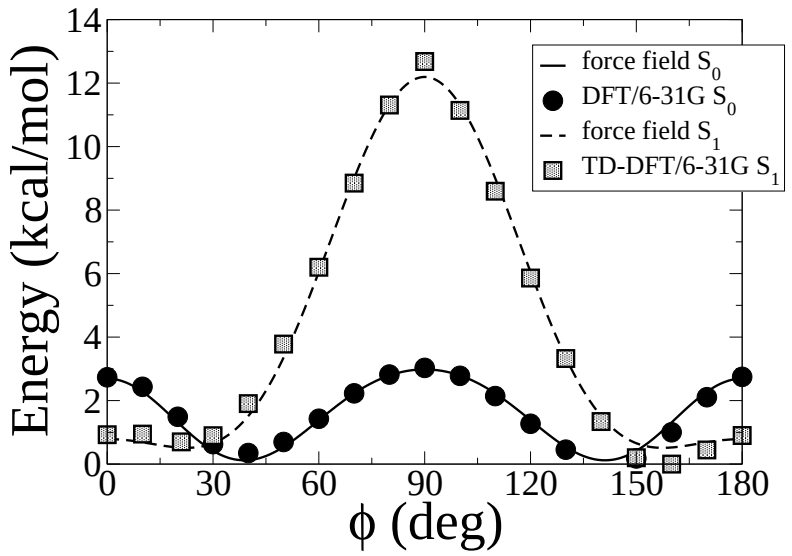

Figure 4: Ground and excited state torsional potential calculated at the B3LYP level using the 6-31G basis set; ϕ is the torsional dihedral angle.

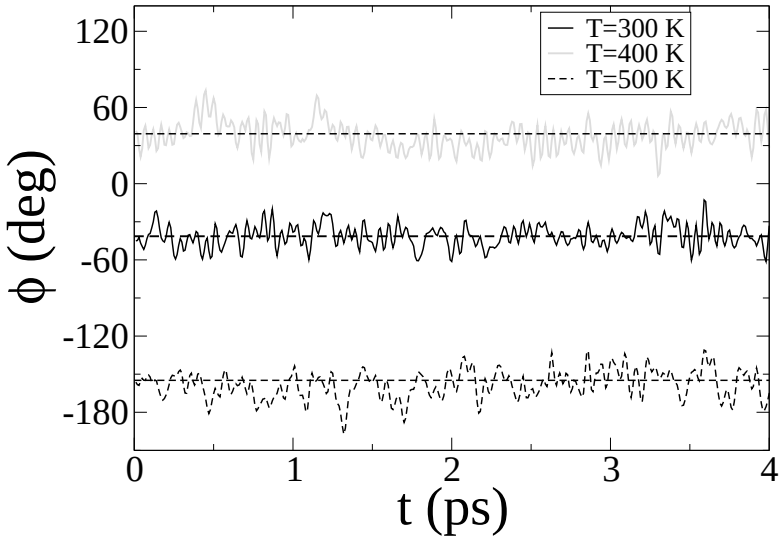

Figure 5: The intramolecular torsional dihedral angle ϕ as function of time t for different temperatures.

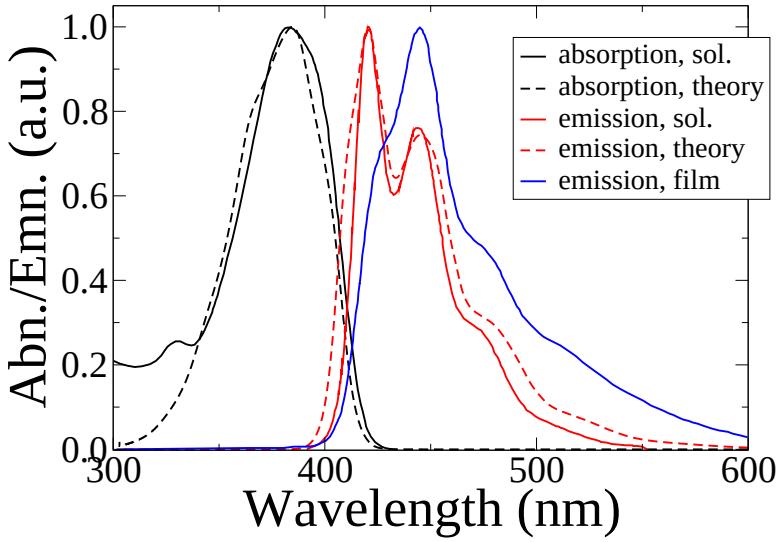

Figure 6: Simulated absorption (black dashed line) and emission (red dashed line) spectra as well as room temperature experimental absorption (black solid line) and emission (red solid line) spectra in toluene and K_2CO_3 solution.[10] Emission spectrum for an IF3 film, drop-casted from solution,[10] is also shown with a blue solid line.

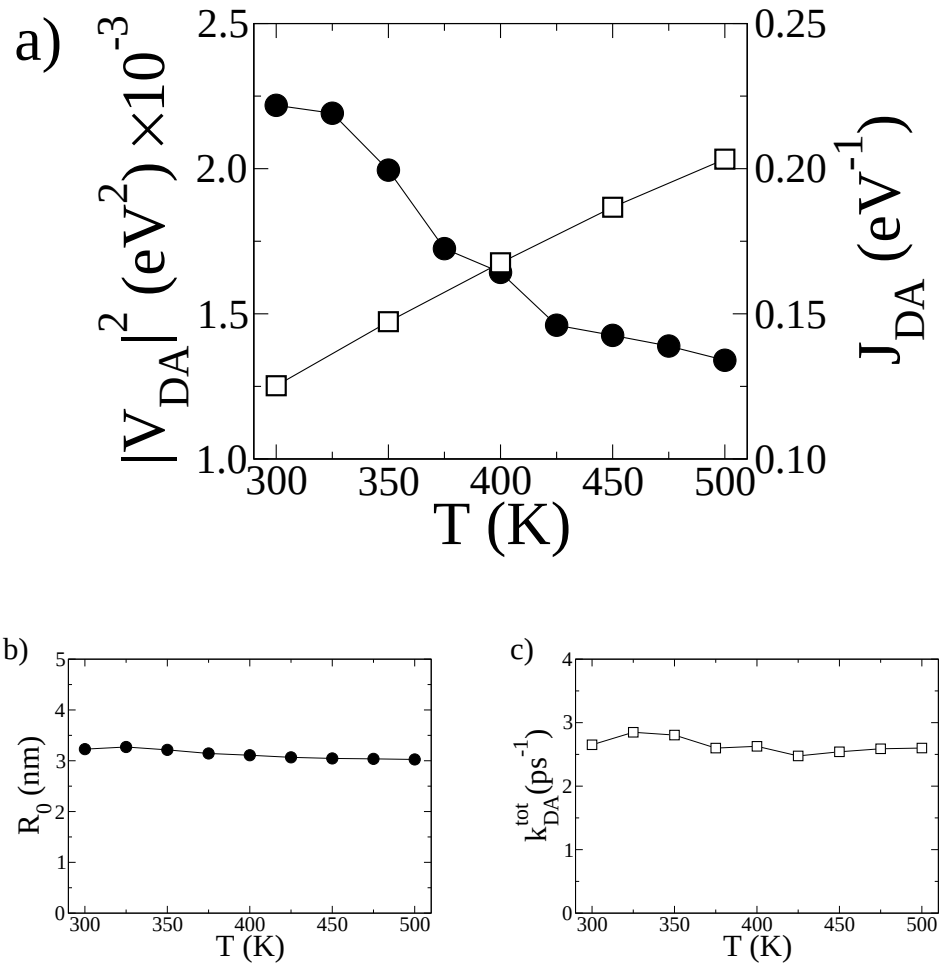

Figure 7: a) The total squared electronic coupling $|V_{DA}|^2$ (circles) and spectral overlap J_{DA} (squares) as a function of absolute temperature T. The Förster radius R_0 (b) and the total hopping rate k_{DA}^{tot} (c) as a function of T.

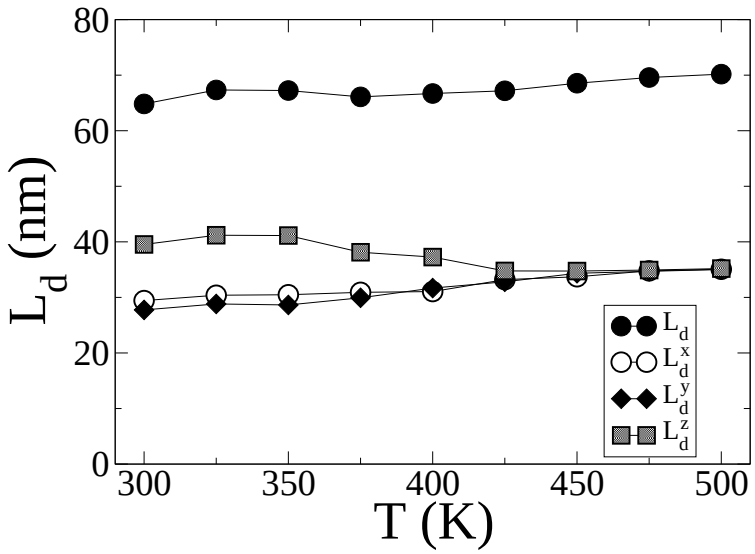

Figure 8: The x, y, z components of the diffusion length (L_d^x, L_d^y and L_d^z respectively) as a function of T.

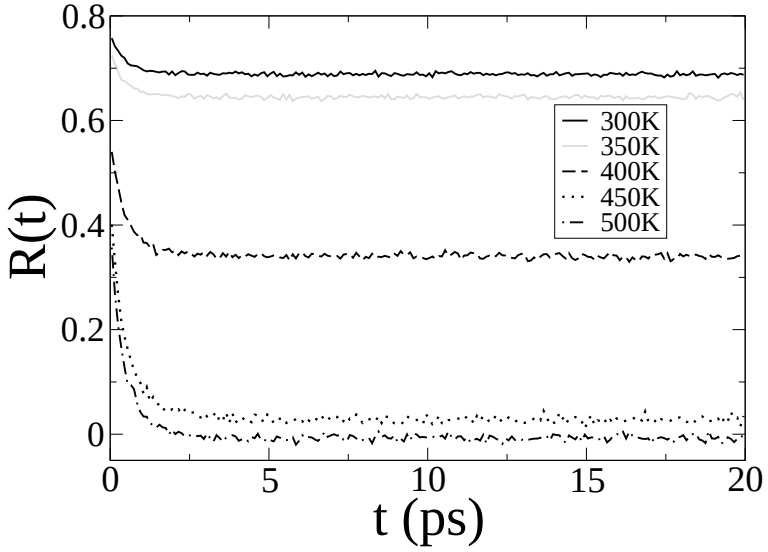

Figure 9: The fluorescence anisotropy ratio $r(t) = (I_{\parallel} - I_{\perp})/(I_{\parallel} + 2I_{\perp})$ as a function of time and temperature Replace R with r on the y axis.

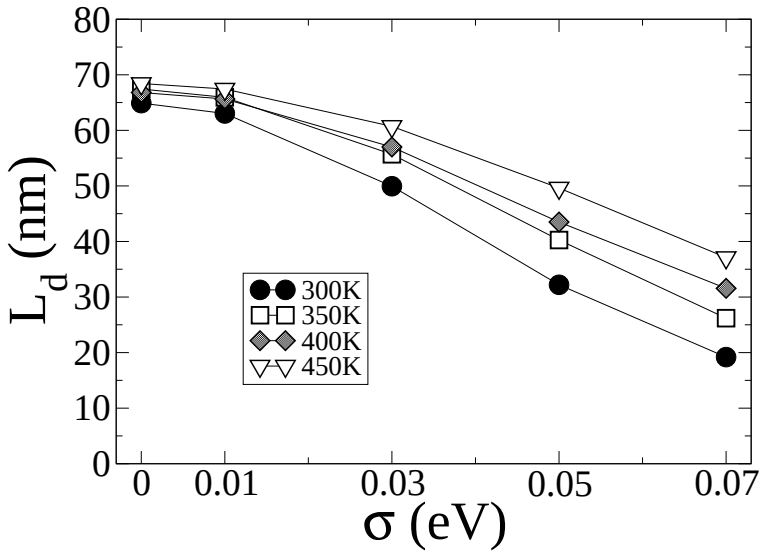

Figure 10: The diffusion length L_d as a function of the energetic disorder width parameter σ for various temperatures.

Supporting Information Available

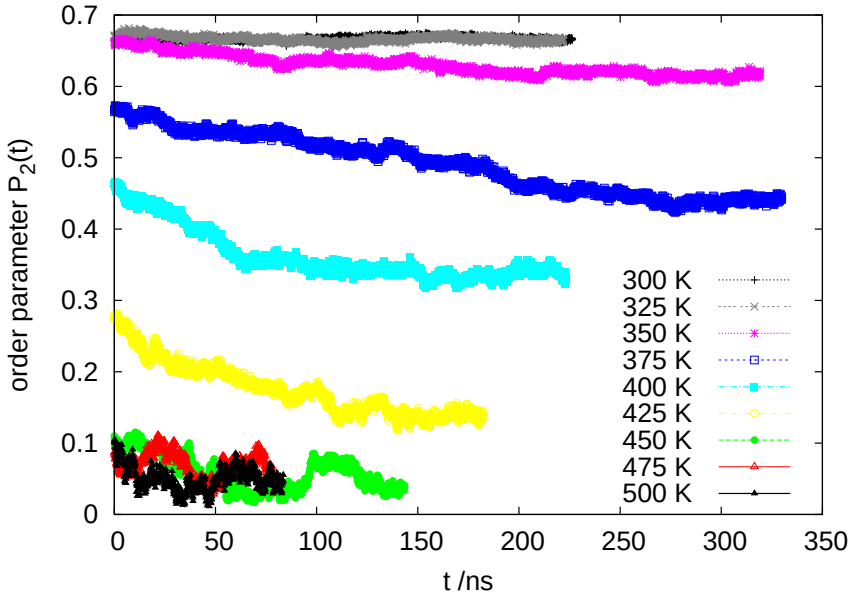

Figure SI 1: Evolution of the nematic order parameter during the equilibration phase of the 256-molecule samples.

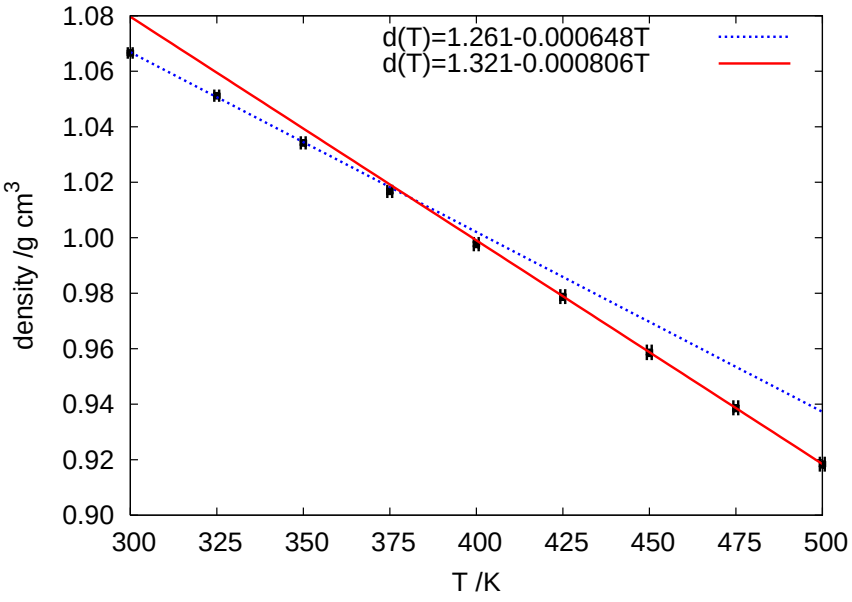

Figure SI 2: Simulated temperature behaviour of the density in the smectic (low T) and isotropic (high T) phase. In each phase, the temperature dependence follows a linear trend; the least square fitting lines and parameters are also reported. The two lines intersect at T=379.7 K

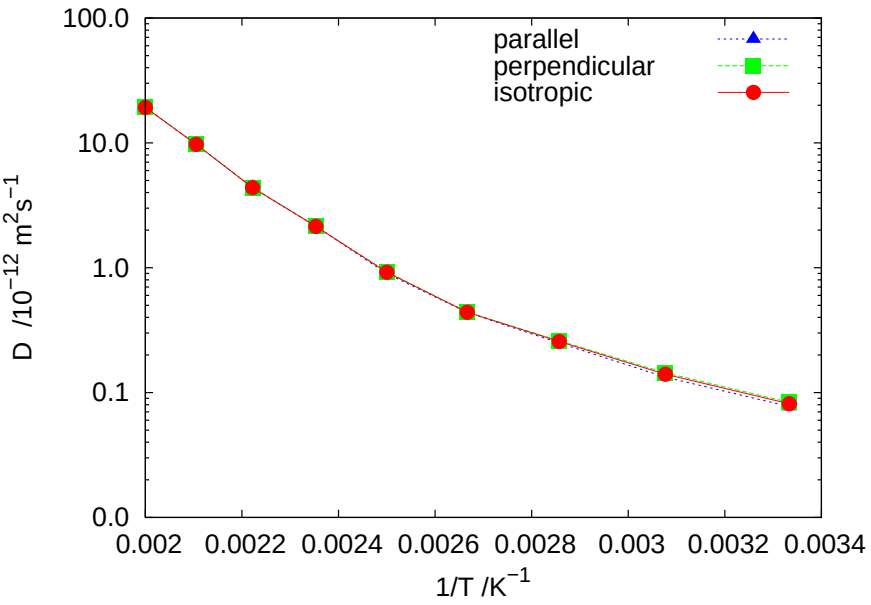

Figure SI 3: Arrhenius plot of the translational diffusion coefficient, calculated from the mean square displacements of the centers of mass ($D_{ii} = \langle [r_i(t) - r_i(0)]^2 \rangle / 2t$, t=10 ns, i=x,y,z, $D_\perp = (D_{xx} + D_{yy})/2$, $D_\parallel = D_{zz}$). The diffusion is fairly isotropic also in the smectic phase, but the phase change is revealed by the two separate regions with different activation energy.

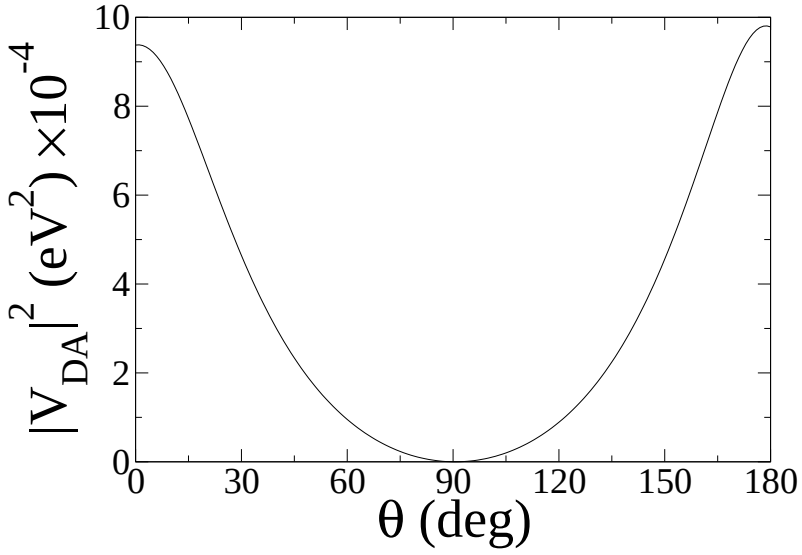

Figure SI 4: The squared excitonic coupling $|V_{DA}|^2$ between two chromophores as a function of their relative orientation and distance of 8.5Å, which corresponds to the average distance between first nearest neighbors within the smectic layers at 300 K.

This material is available free of charge via the Internet at `http://pubs.acs.org`.

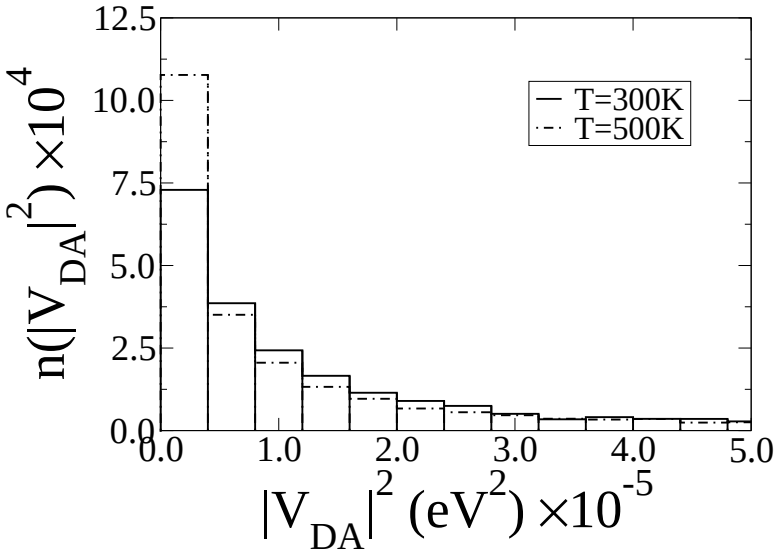

Figure SI 5: The distribution of the squared excitonic coupling $|V_{DA}|^2$ for T=300K and T=500K.

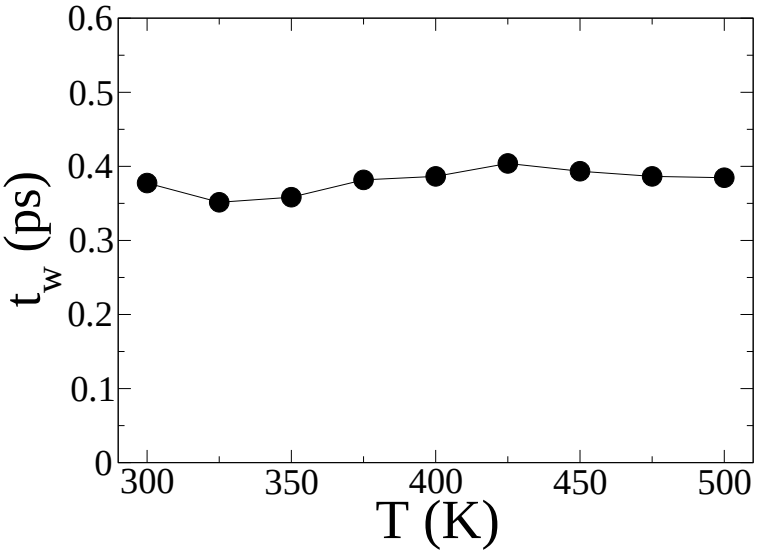

Figure SI 6: The average waiting time of the exciton as a function of temperature.

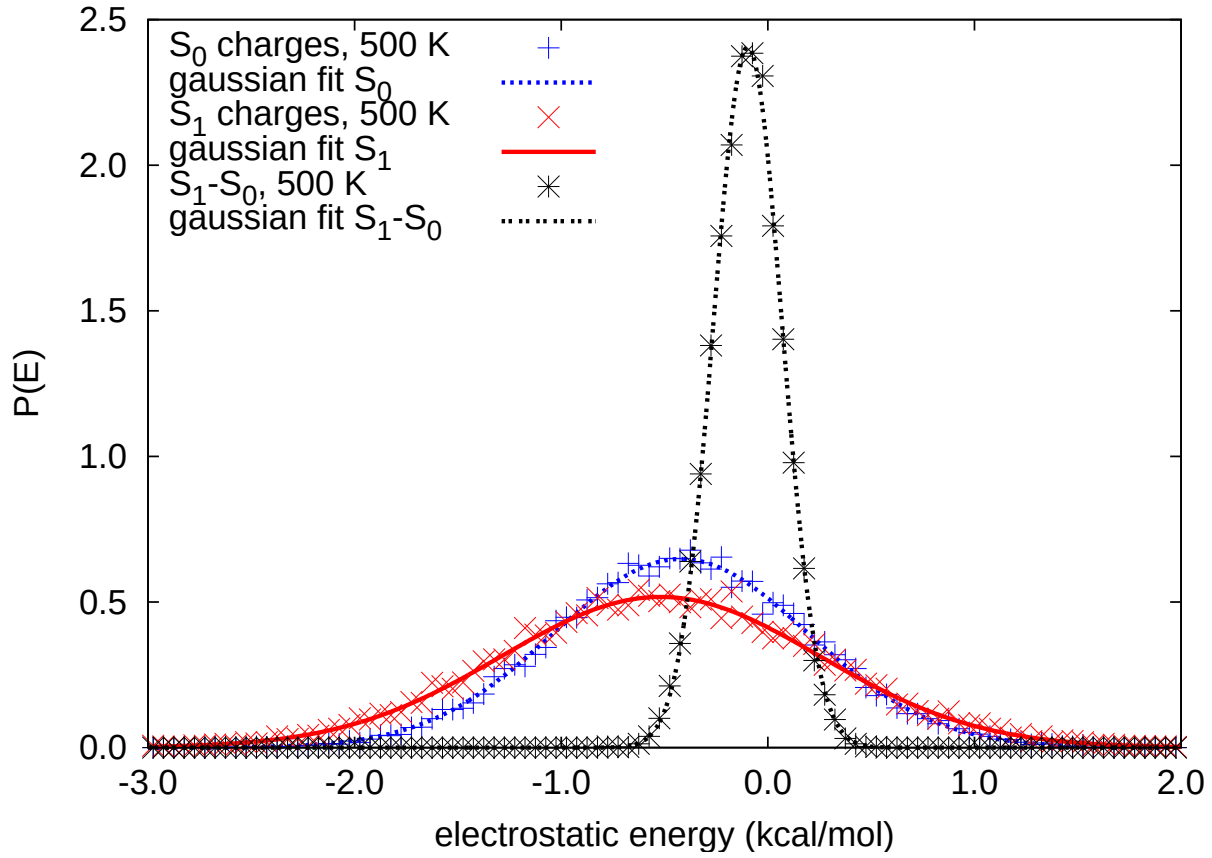

Figure SI 7: The electrostatic disorder distribution at 500 K. The distributions for the ground and excited states correspond to calculation of the electrostatic interaction bewteen a molecule and all its neighbours using the ground state and excited state atomic charges, respectively (. The difference distribution is instead the difference between ground and excited state electrostatic energy calculated for the same molecule. The standard deviations are σ_0 =0.62 kcal/mol (0.0267 ev), σ_1 =0.77 kcal/mol (0.0334 eV), σ_{1-0} =0.166 kcal/mol (0.007 eV). The difference distribution bewteen two arbitrary molecules instead should have standard deviation $\sigma_{1,i-0,j} = (\sigma_1^2 + \sigma_0^2)^{1/2}$ =0.99 kcal/mol (0.0429 eV). All deviations are of the order or even smaller than the thermal energy at 500 K which corresponds to 0.994 kcal/mol (0.04308 eV).

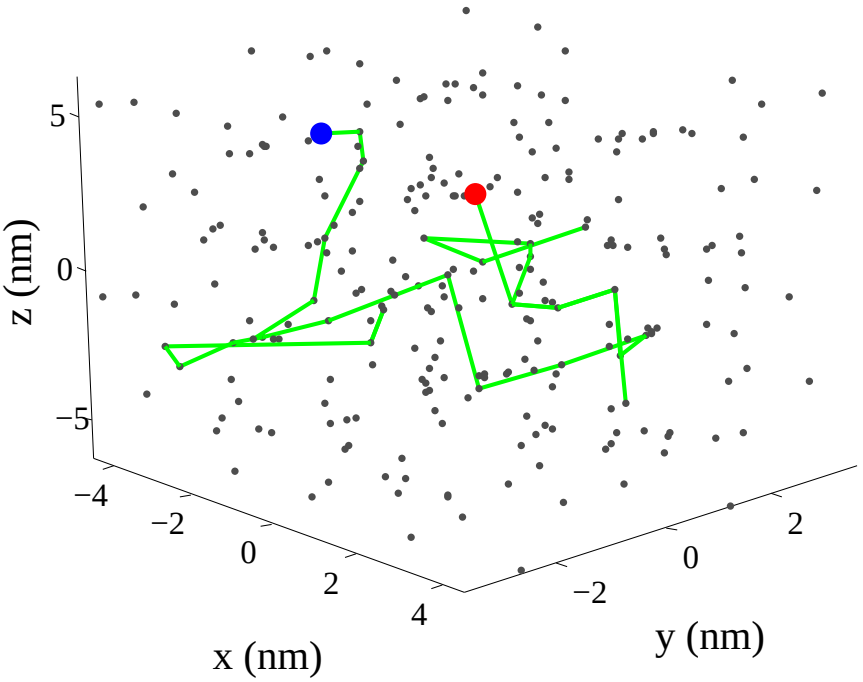

Figure SI 8: A trajectory of an exciton as it hops from the site of creation (blue) until the site where it recombines (red).